Post- print of: R. Ryndzionek, Ł. Sienkiewicz, M. Ronkowski, M. Michna, F. Kutt and G. Kostro, "FEA analysis of the multicell piezoelectric motor," IECON 2019 - 45th Annual Conference of the IEEE Industrial Electronics Society, Lisbon, Portugal, 2019, pp. 796-801, doi: 10.1109/IECON.2019.8927522.

FEA analysis of the multicell piezoelectric motor

1st Roland Ryndzionek
Gdansk University of Technology
Faculty of Electrical and Control Engineering
Gdansk, Poland
roland.ryndzionek@pg.edu.pl

2nd Łukasz Sienkiewicz
Gdansk University of Technology
Faculty of Electrical and Control Engineering
Gdansk, Poland
lukasz.sienkiewicz@pg.edu.pl

3rd Mieczysław Ronkowski
Gdansk University of Technology
Faculty of Electrical and Control Engineering
Gdansk, Poland
mieczyslaw.ronkowski@pg.edu.pl

4th Michal Michna
Gdansk University of Technology
Faculty of Electrical and Control Engineering
Gdansk, Poland
michal.michna@pg.edu.pl

5th Filip Kutt
Gdansk University of Technology
Faculty of Electrical and Control Engineering
Gdansk, Poland
filip.kutt@pg.edu.pl

6th Grzegorz Kostro
Gdansk University of Technology
Faculty of Electrical and Control Engineering
Gdansk, Poland
grzegorz.kostro@pg.edu.pl

***Abstract*— The presented paper concerns a design, modeling and chosen tests of the prototype multicell piezoelectric motor (MPM). The principle of operation based on three independent traveling wave actuators is presented. The main materials and technologies used in the fabrication process are described. The structure of the motor is modeled using static and modal FEM analysis. The process of traveling wave generation in the MPM structure is demonstrated. Finally, the main results of the simulation are validated by measurements of MPM prototype. The natural frequencies of three actuators are measured along with the corresponding displacements at two locations.**

***Keywords*— Piezoelectricity, Piezoelectric transducers, Traveling wave devices, Piezoelectric resonators, Simulation, Piezoelectric actuators, Piezoelectric motors**

I. Introduction

Over the last few decades a big improvement has been made in the analysis and design process of electrical machines, actuators and sensors, mainly due to improved computer capabilities and advancements in material engineering [1]–[4]. Significant progress in the field of materials engineering gives an opportunity to develop new electromechanical structures with various configurations and topologies [5]–[8]. In recent years, an increasing interest in so-called magnetoelectric multiferroics was observed. The researchers are working still to optimize the desirable properties of the above materials, a chemical modification of the initial formula is often used [9], [10].

Besides "classic" electric motors there are other interesting solutions using unconventional topologies. One of them is a piezoelectric motor concept, a bit forgotten recently. However, the aforementioned development of materials still gives new possibilities of improvement to the properties of systems [11], [12]. Moreover, as presented in Fig. 1, the comparison of performances of various electromechanical conversion mechanisms clearly shows the potential of novel electroactive materials. The Y-axis describes specific driving efforts of transducers. It is the ability to produce the effort in terms of volume. The X-axis describes a relative speed of deformation. It represents the speed at which the transducer's active part can be deformed and go back to its bulk. The product of these two quantities gives the theoretical power density [13].

Piezoelectricity is widely used in industrial sectors such as the production and detection of sound, generation of high voltages, electronic frequency generation, microbalances, bio-medical sensors, driving an ultrasonic nozzle and ultrafine focusing of optical assemblies [14], [15].

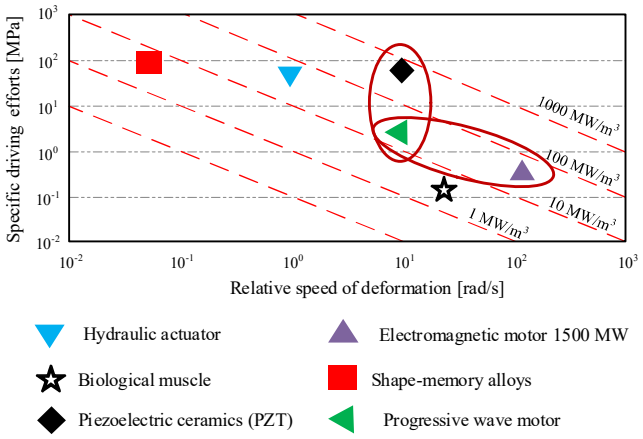

Fig. 1 Comparison of transducer technologies **[16], [17]**.

Those systems are characterized by a high functional integration level and high performance. It should be stressed that this depends essentially on the possibility of generating high specific efforts in a very limited volume of mass, i.e., driving constraints are up to the order of 40 MPa in the PZT piezoelectric ceramics, or to the order of 100 MPa in the shape memory alloys.

Piezoelectricity is a form of coupling between the mechanical and electrical phenomenon. There are two piezoelectric effects - direct and the converse piezoelectric effects (Fig. 2). In 1881 Pierre and Jacques Curie discovered the direct piezoelectric effect. A year later, relying on the work of Lippmann, they demonstrated the converse effect. The direct piezoelectric effect occurs when mechanical force or pressure is applied to piezoelectric material and the electric charge or voltage is induced on the surface (as can be seen in Fig. 2a). Conversely, if some charge or voltage is applied on a piezoelectric material, then the mechanical force and strain are generated (Fig. 2b) [18], [19].

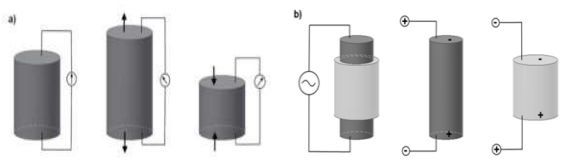

Fig. 2 The piezoelectric effect: a) the direct piezoelectric effect, b) the converse piezoelectric effect.

The main purpose of this paper is the validation of the finite element method (FEM) analysis results by measurements of multicell piezoelectric motor (MPM) prototype. FEM is used to compute the resonance frequencies and displacements of three transducers on the stator. The performance of the MPM prototype is assessed by laser vibrometry measurement (detecting of resonance frequencies and maximal displacements) and compared with the simulation.

II. MPM CONCEPT

The concept of the MPM is based on a combination of two topologies: traveling wave motor/actuator, and the rotating-mode motor/actuator [20]. The active part of the MPM is the stator containing three actuators. The electromechanical structure of each rotating mode actuator is considered as an independent "single cell". Every single cell deforms due to the voltage applied to the piezoelectric ceramics (PZT) at the frequency corresponding to two bending eigenmodes. Superposition of those modes creates a traveling wave motion at the actuator's surface. PZTs are disc-shaped and they form a stack, with disc's rotation of 90° between two pairs. Each cell is prestressed by a screw. Due to the symmetrical structure of the actuators, the second rotor can be used. This should lead to increased output quantities of the MPM such as torque and speed. The counter-mass (part of the stator) is made from aluminum alloy AU4G type, to reduce the weight of the actuator. Moreover, this material allows for the reduction of mechanical losses compared to steel. The rotors are made of steel, as a material of high density was a design requirement. The full assembly of the MPM is presented in Fig. 3. A more detailed description has been presented in [21].

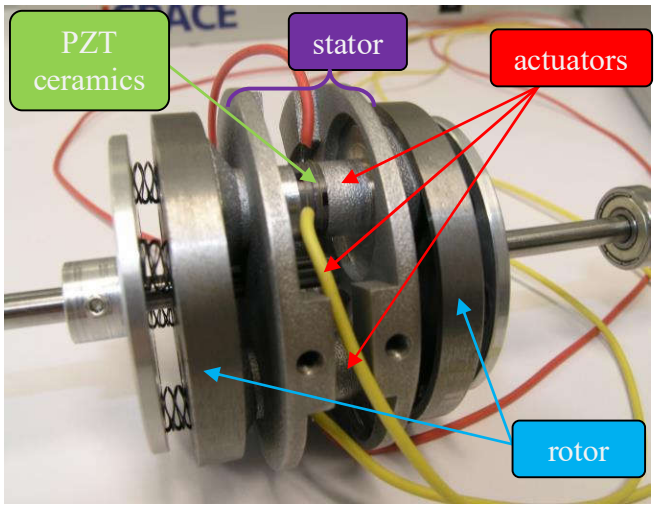

Fig. 3 The full assembly view of the MPM prototype.

III. FEM ANALYSIS

Finite Element Method analysis is divided into two parts. The first one is the simulation of the piezoceramic rings to determine the displacement directions as well as a demonstration of traveling wave generation on the actuator's surface. The second part is dedicated to the static and modal analysis of the whole structure of the MPM.

Four piezoelectric ceramics have been created and connected to generate the traveling wave. Each ceramic is divided into halves with opposite polarization. As stated in the previous chapter, two pairs of ceramics are rotated by 90° to each other. The ceramic dimensions are as follows: external diameter - 12.5 mm, internal diameter - 5 mm and thickness - 1 mm. For the individual discs to work as a stack it is necessary to lock the degrees of freedom in the contact surfaces. The piezoelectric material used in the analysis is hard-doped PZT 189 manufactured by Quartz and Silice. The main material properties are presented in Table 1.

TABLE I. PROPERTIES OF PIEZOELECTRIC CERAMIC USED IN THIS WORK (QUARTZ & SILICE PZT189)

PARAMETER	SYMBOL	MODEL VALUE
RELATIVE DIELECTRIC CONSTANT	$\varepsilon^{T}_{33}/\varepsilon_0$	1020
ELECTROMECH. COUPLING FACTORS	k_{31}	0.30
	k_{33}	0.69
	k_{15}	0.47
PIEZOELECTRIC CHARGE CONSTANT	d_{31}	-100
	d_{33}	-250
QUALITY FACTOR	Q_M	1000
DENSITY	ϱ	7600

A. *Piezoelectric ceramics analysis*

The generated mesh of the piezoelectric stack is presented in Fig. 4. The precision of the simulation depends on the mesh density and mesh form. It is crucial to get an equal shape of the elements. In the case of ring-shaped geometry, the use of the automatic mesh generator gave satisfactory results. The analysis of the piezoelectric stack is computed to verify if the traveling wave is generated on its surface. Two sinusoidal voltage sources with phase shift are applied to each pair of ceramics. One working cycle of the traveling wave propagation has been presented in Fig. 5. Depending on the presented step, half of the piezoelectric ceramic is shrinking or extending. Finally, as a result of the appropriate synchronization, the traveling wave is generated on the surface. Colored arrows are demonstrating the rotary motion (Fig. 5).

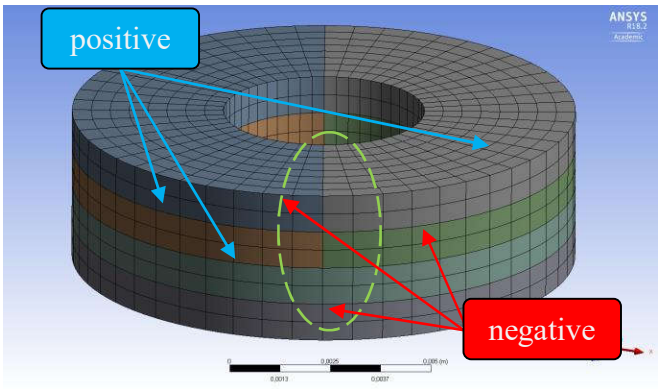

Fig. 4 Piezoceramic stack geometry and mesh generated in the FEM software. The green circle is the section presented in Fig. 5.

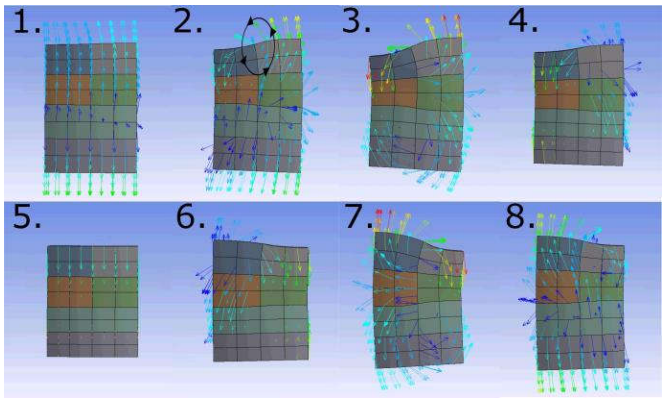

Fig. 5 The traveling wave generation principle in the piezoelectric ceramics stack. Red arrows indicate the biggest deflections and blue arrows indicate the smallest deflections.

The total displacement is presented in Fig. 6 which corresponds to step 7 in Fig 5. As expected the biggest displacements occur on the edges of ceramics.

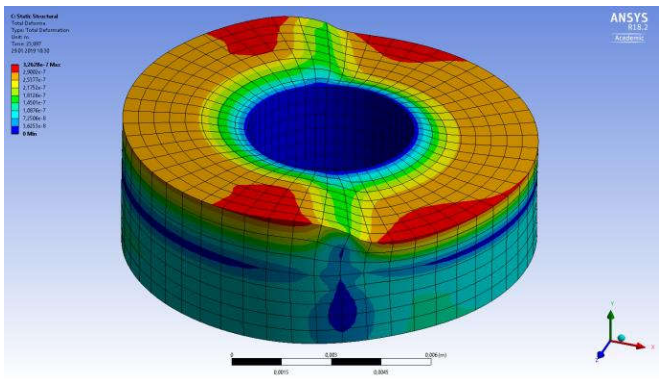

Fig. 6 Results of static FEM analysis: the maximal displacement of the piezoelectric stack.

The small displacements (single µm range) produced by the piezoelectric ceramics need to be amplified by the resonance of the mechanical structure of the stator.

B. Stator (mechanical structure) analysis

The next stage of FEM analysis included simulation of MPM's full structure. This was divided into two parts – modal (resonance analysis of the structure) and static (displacement analysis under DC voltage excitation).

The main goal of a modal analysis is to obtain the resonance frequency of actuators higher than 20 kHz, which is in the ultrasonic range. The results of a modal analysis have shown that several modes are observed in a 20 kHz - 100 kHz frequency range. However only two frequencies are useful in terms of traveling wave generation – 25 400 kHz and 26 015 kHz (Fig. 7) – which correspond to bending modes. Other resonance frequencies are linked with respiration modes or with deformations of the armature.

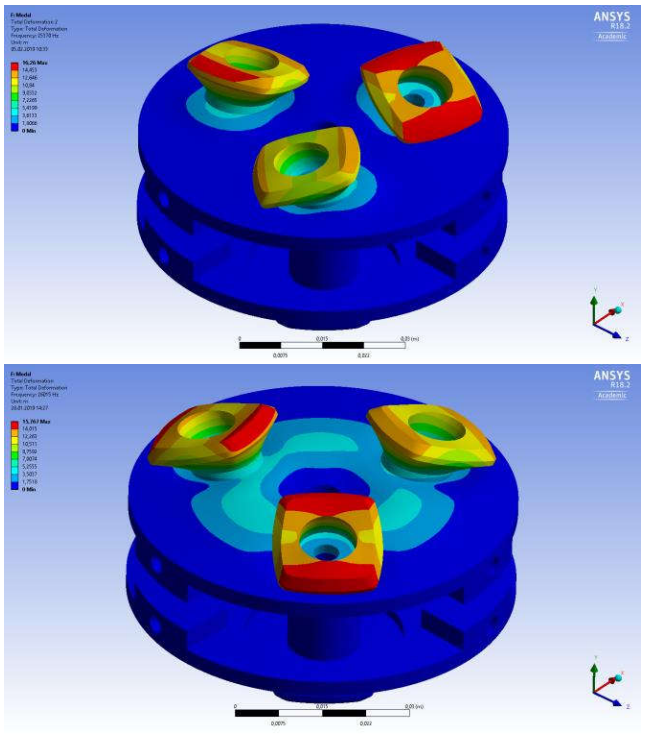

Fig. 7 Results of modal FEM analysis: bending displacement of the actuators at the resonance frequencies of 25400 (upper half) and 26015 Hz (lower half).

The main goal of the static structural simulation is to determine the displacements in the stator structure generated by the traveling wave on the ceramics and verify its value.

The ceramics are supplied by two sinusoidal voltages with a peak-to-peak value of 400V and 90° phase shift. The external and internal diameter surface of the stator is fixed. The AU4G alloy material is assigned to the counter-masses. The simulation results are presented in the following figures: Fig. 8, Fig. 9 and Fig. 10. The contact surface between the rotor and stator is where maximal deflections are present. More precisely they occur on the edges of each actuator in the counter-mass. That is the desired behavior because the rotor is driven by friction. Those points, at the rotor/stator contact surface, are oscillating according to an elliptic trajectory. Moreover, the movement of three actuators on the stator (Fig. 8-10) corresponds to the displacement of the ceramics shown in Fig. 5, steps no. 3, 5 and 7. The maximum simulated deflection is 2.6 µm.

Besides the edges of the actuator, the second interesting region is the surface around the actuator. In this area, the parasitic displacement appears. The simulated displacement has an amplitude of 0.7 µm (Fig. 8). Parasitic displacements should be reduced because they may cause degradation of the material.

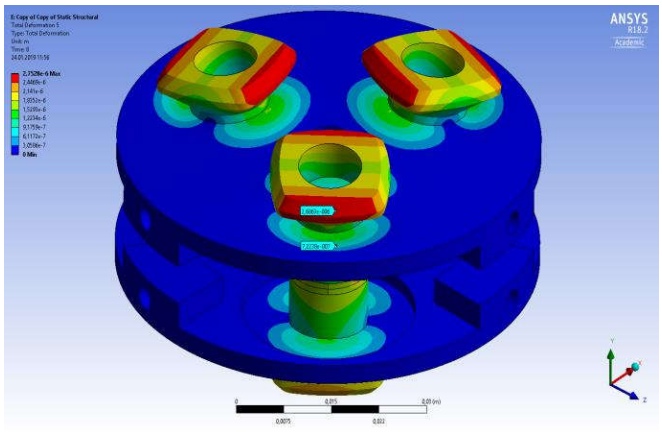

Fig. 8 Results of static FEM analysis: the first step in traveling wave generation in stator - maximum displacement at the external edges of actuators. Corresponding displacement of the ceramics (Fig. 5, step no. 3).

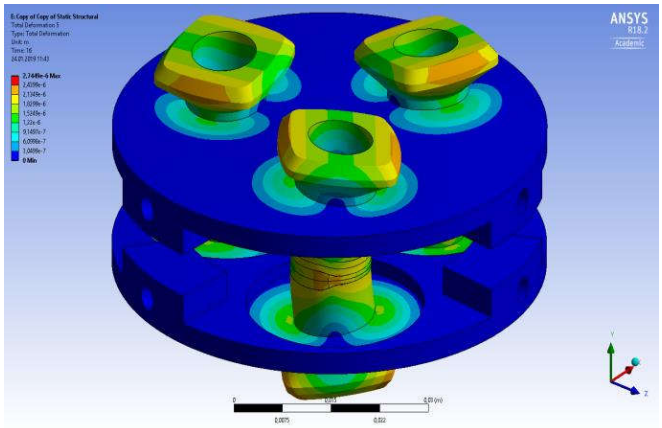

Fig. 9 Results of static FEM analysis: the second step in traveling wave generation in stator - neutral position of the actuators. Corresponding displacement of the ceramics (Fig. 5, step no. 5).

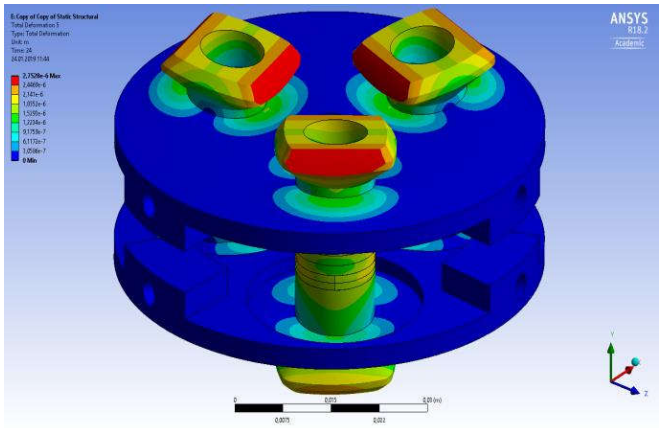

Fig. 10 Results of static FEM analysis: the third step in traveling wave generation in stator - maximum displacement at the internal edges of actuators. Corresponding displacement of the ceramics (Fig. 5 step 7).

IV. Experimental Analysis

The aim of this stage of MPM study is a validation of FEM analysis results described in the previous chapter. The experimental analysis includes measurements of the resonance frequencies and displacements of the MPM's structure. At first, the MPM prototype is assembled. The crucial part of the process is a fine-tuning of the actuators. By tightening of screws which connect the stack of ceramics with the counter-masses one can change the applied force. The actuator's frequency of resonance changes as a consequence. The final frequencies measured in each actuator are 24.26 kHz, 24.23 kHz, and 24.09 kHz. The measurement is done thanks to Agilent 4294A impedance analyzer. The Bode plot of the chosen actuator is shown in Fig. 11. In comparison with the FEM analysis results (bending mode at 25.4 kHz), the resonance frequencies are similar (in terms of ultrasonic piezoelectric motors). That proves the validity of the proposed numerical model.

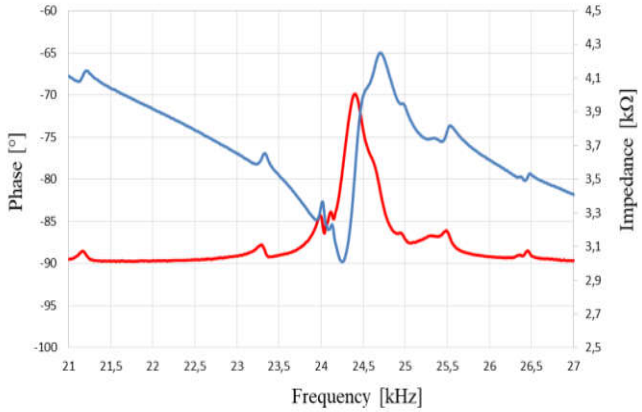

Fig. 11 Bode plot measured for one of the actuators, where the red line is impedance and the blue line is a phase shift.

The next step of the analysis is the measurement of displacement at the stator's surface. The measurement at point A is made on the surface which comes into contact with the rotor. A measurement at point B is made on the stator armature, near the placement of the actuator. The amplitude of vibration is measured by a Polytec CLV laser vibrometer system (Fig. 12).

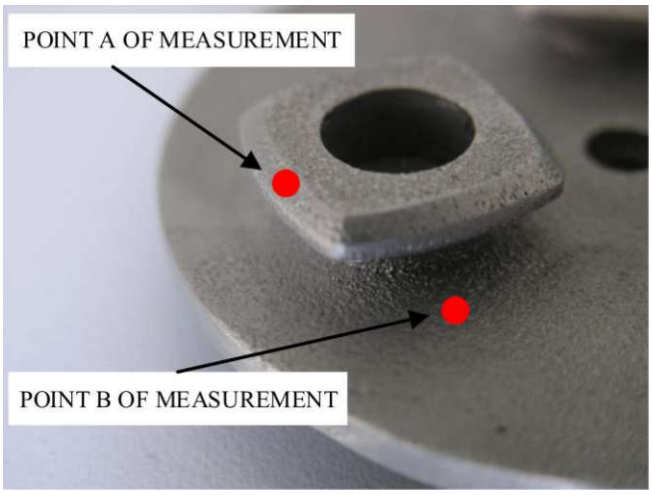

Fig. 12 Points of measurement for the laser's head.

The measured displacements at points A and B are presented in Fig. 13. The values of sinusoidal displacements at point A and B are 2.2 µm and 0.65 µm (peak-to-peak), respectively. The latter value is decreasing if the distance between point B and the actuator is increasing. In comparison with the FEM analysis results (2.6 µm and 0.7 µm respectively), the measured displacement values can be considered as satisfactory. Moreover, the measured displacement waveforms are sinusoidal, as it was required.

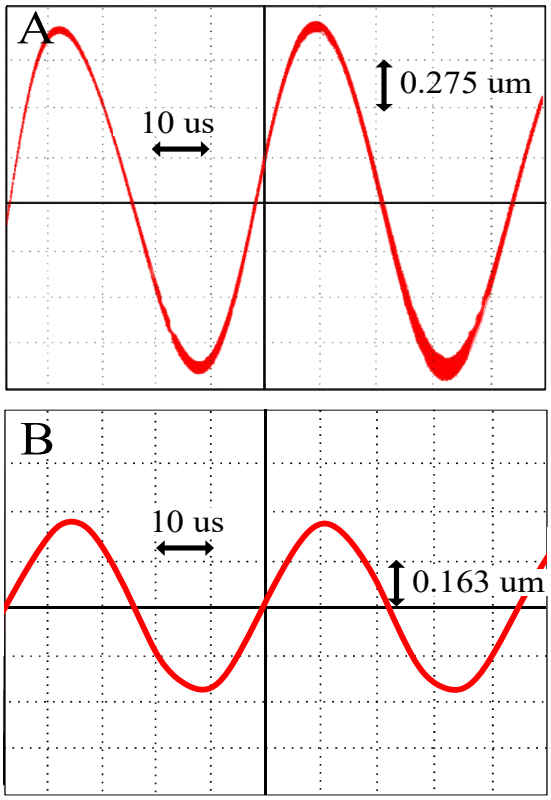

Fig. 13 Displacement measurements at point A and at point B (frequency of resonance f =24.26 Hz).

V. Conclusions

In this paper, the concept of a multicell piezoelectric motor, FEM and experimental analysis have been presented. The FEM analysis has been carried out in the ANSYS environment (Workbench) to determine the resonance frequencies and the displacements in the stator structure. Finally, a prototype of MPM has been manufactured and tested in the laboratory (Fig. 14). The results of FEM analysis have been compared with the measurement results. The numerical model has been validated with satisfying accuracy and provides useful perspectives for further MPM study and design.

The future research works are associated with the optimization of the manufactured MPM prototype and verification of its loading limits.

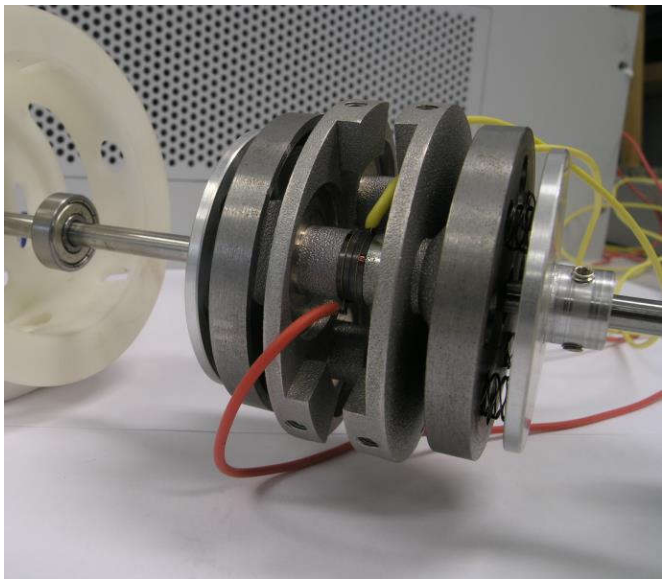

Fig. 14 The prototype of MPM with housing.

Acknowledgment

Authors express gratitude towards MESCO, an authorized distributor of ANSYS, for granting the Workbench license.

References

[1] R. Pałka and R. Piotuch, "Experimental verification of Dead-Beat predictive current controller for small power, low speed PMSM," *Arch. Electr. Eng.*, vol. Vol. 67, no. nr 2, pp. 333–-343, 2018.

[2] F. Wilczyński, M. Morawiec, P. Strankowski, J. Guziński, and A. Lewicki, "Sensorless field oriented control of five phase induction motor with third harmonic injection," in *2017 11th IEEE International Conference on Compatibility, Power Electronics and Power Engineering (CPE-POWERENG)*, 2017, pp. 392–397.

[3] F. Morel, X. Lin-Shi, J. Retif, B. Allard, and C. Buttay, "A Comparative Study of Predictive Current Control Schemes for a Permanent-Magnet Synchronous Machine Drive," *IEEE Trans. Ind. Electron.*, vol. 56, no. 7, pp. 2715–2728, Jul. 2009.

[4] M. Morawiec, P. Strankowski, A. Lewicki, J. Guzinski, and F. Wilczynski, "Feedback Control of Multiphase Induction Machines with Backstepping Technique," *IEEE Trans. Ind. Electron.*, pp. 1–1, 2019.

[5] C. H. Cheng and S. K. Hung, "A Piezoelectric Two-Degree-of-Freedom Nanostepping Motor With Parallel Design," *IEEEASME Trans. Mechatron.*, vol. 21, no. 4, pp. 2197–2199, Aug. 2016.

[6] J. Li *et al.*, "Development of a Novel Parasitic-Type Piezoelectric Actuator," *IEEEASME Trans. Mechatron.*, vol. 22, no. 1, pp. 541–550, Feb. 2017.

[7] L. Petit, R. Briot, L. Lebrun, and P. Gonnard, "A piezomotor using longitudinal actuators," *IEEE Trans. Ultrason. Ferroelectr. Freq. Control*, vol. 45, no. 2, pp. 277–284, Mar. 1998.

[8] M. Morawiec, "Z-Type Observer Backstepping for Induction Machines," *IEEE Trans. Ind. Electron.*, vol. 62, no. 4, pp. 2090–2102, Apr. 2015.

[9] M. Podgórna, M. Ptak, M. Chrunik, I. Jankowska-Sumara, J. Piecha, and D. Zasada, "The investigations of phase transitions in the (1-x)PbZrO3-xBiFeO3 nanocrystals using differential scanning calorimetry and Raman spectroscopy," *J. Appl. Phys.*, vol. 124, no. 5, p. 054102, Aug. 2018.

[10] D. Węgłowska, P. Perkowski, M. Chrunik, and M. Czerwiński, "The effect of dopant chirality on the properties of self-assembling materials with a ferroelectric order," *Phys. Chem. Chem. Phys.*, vol. 20, no. 14, pp. 9211–9220, Apr. 2018.

[11] A. D. Ledbetter, H. N. Shekhani, M. M. Binkley, and J. M. Meacham, "Tuning the Coupled-Domain Response for Efficient Ultrasonic Droplet Generation," *IEEE Trans. Ultrason. Ferroelectr. Freq. Control*, vol. 65, no. 10, pp. 1893–1904, Oct. 2018.

[12] U. Bachulska, J. Jankowska-Sumara, A. Majchrowski, M. Chrunik, D. Zasada, and A. Soszyński, "Thermal and dielectric properties of ferroelectric lead germanate single crystals doped with chromium ions

(Pb5Ge3O11:Cr3+)," *Phase Transit.*, vol. 91, no. 9–10, pp. 923–931, Oct. 2018.
[13] B. Nogarede, C. Henaux, and J.-F. Rouchon, "Actionneurs électromécaniques pour la robotique et le positionnement - Fondamentaux et structures de base," *Ref : TIP302WEB - "Réseaux électriques et applications,"* 10-Nov-2008. [Online]. Available: https://www.techniques-ingenieur.fr/base-documentaire/energies-th4/applications-electromecaniques-42268210/actionneurs-electromecaniques-pour-la-robotique-et-le-positionnement-d5341/. [Accessed: 23-Jan-2019].
[14] T. Mashimo, S. Toyama, and H. Ishida, "Design and implementation of spherical ultrasonic motor," *IEEE Trans. Ultrason. Ferroelectr. Freq. Control*, vol. 56, no. 11, pp. 2514–2521, Nov. 2009.
[15] L. Sienkiewicz, M. Ronkowski, G. Kostro, R. Ryndzionek, and J. F. Rouchon, "Identification of the mechanical properties of the skin by electromechanical impedance analysis of resonant piezoelectric actuator," in *IECON 2013 - 39th Annual Conference of the IEEE Industrial Electronics Society*, 2013, pp. 3940–3945.
[16] B. Nogarede, "Moteurs piézoélectriques," *Tech. Ing.*, vol. D3765 V1, 1996.
[17] B. Nogarede, J.-F. Rouchon, and A. Renotte, "Electroactive Materials: Toward Novel Actuation Concepts," in *Recent Developments of Electrical Drives*, Springer Netherlands, 2006, pp. 435–442.
[18] B. Nogarede, C. Henaux, and J.-F. Rouchon, "Actionneurs électromécaniques pour la robotique et le positionnement - Fondamentaux et structures de base," *Tech. L'Ingenieur*, 2008.
[19] W. M. Jayarathne, W. A. T. Nimansala, and S. U. Adikary, "Development of a Vibration Energy Harvesting Device Using Piezoelectric Sensors," in *2018 Moratuwa Engineering Research Conference (MERCon)*, 2018, pp. 197–202.
[20] M. Budinger, J. F. Rouchon, and B. Nogarede, "Analytical modeling for the design of a piezoelectric rotating-mode motor," *IEEEASME Trans. Mechatron.*, vol. 9, no. 1, pp. 1–9, Mar. 2004.
[21] R. Ryndzionek, M. Michna, M. Ronkowski, and J. Rouchon, "Chosen Analysis Results of the Prototype Multicell Piezoelectric Motor," *IEEEASME Trans. Mechatron.*, vol. 23, no. 5, pp. 2178–2185, Oct. 2018.